VELOCITY DERIVATIVES IN TURBULENT FLOW FROM 3D-PTV MEASUREMENTS

Beat Lüthi, Ulrich Burr, Albert Gyr, Wolfgang Kinzelbach
Institut für Hydromechanik und Wasserwirtschaft, ETH-Hönggerberg
CH-8093, Zürich, Switzerland
luethi@ihw.baug.ethz.ch

Arkady Tsinober
Faculty of Engineering, Tel Aviv University
69974, Tel Aviv, Israel
tsinober@eng.tau.ac.il

ABSTRACT

Velocity derivatives play an outstanding role in the dynamics of turbulence for a number of reasons. Their importance became especially clear since the papers by Taylor (1938) and Kolmogorov (1941). Taylor emphasized the role of vorticity, whereas Kolmogorov stressed the importance of dissipation, and thereby of strain.

The field of velocity derivatives is very sensitive to the non-Gaussian nature of turbulence or more generally to its structure, and hence reflects a lot of its physics. From the momentum equation it follows that the whole flow field is entirely determined by the field of vorticity, or by that of strain. Therefore, in Lagrangian description, in a frame following a fluid particle, everything happening in its proximity is characterized by the velocity gradient tensor $A_{ij} = \partial u_i/\partial x_j$ (Tsinober, 2001).

We report the first attempts to use the particle tracking technique for studying the field of velocity derivatives and material elements. The nonintrusive nature of this method makes it especially suitable for this purpose.

FACILITY AND METHOD

A quasi-isotropic turbulent flow field is produced inside a $320 \times 320 \times 175mm^3$ water tank (figure 1). Two 4 by 4 arrays of cylindrical rare earth sintered strong permanent magnets ($42mm$ in diameter) were mounted on the two opposite side walls of the tank. The magnets are arranged in such a way that positive and negative magnetic fluxes alternate, forming a chessboard pattern. Copper plates placed in front of each array serve as

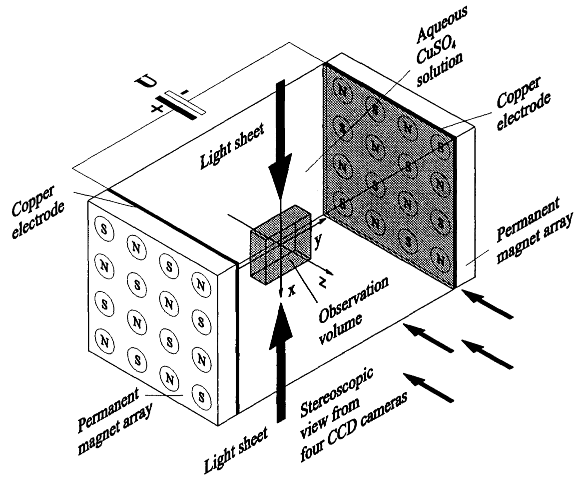

Figure 1: Schematic of the experimental facility and coordinate system (x, y, z).

electrodes. The tank is filled with an aqueous copper sulphate ($CuSO_4$) test fluid. A DC electric current of $9A$ is applied and from the interaction of the current density, $\mathbf{j}$, with the magnetic field, $\mathbf{B}$, Lorentz forces, $\mathbf{f}_l$, are induced, according to $\mathbf{f}_l = \mathbf{j} \times \mathbf{B}$. They produce a non-oscillating swirling motion in the proximity of each magnet. Within a few seconds these circulations cause a three dimensional (3D) time dependent flow region with a front that quickly propagates towards the center resulting in a turbulent velocity field with zero mean flow and fluctuations, u_i, of order $O(0.01m/s)$, occupying the entire volume of the tank. The flow is seeded with neutrally buoyant particles of 40-60 microns in diameter. Four synchronized video cameras with a resolution of 480×640 pixels^2 are focused on a volume of $15 \times 20 \times 20mm^3$ and record frames at a rate of $30Hz$ over a time interval $\tau = 30\,\text{sec}$. A three dimensional **P**article **T**racking **V**elocimetry (3D-PTV) analysis of the images, extensively described in Stüer et al. (1999), determines the position of each particle using a stereometric method and links particles of consecutive images to trajectories.

From the 3D-PTV we get velocities, $\mathbf{u}$, and Lagrangian accelerations, $\mathbf{a}$, at random particle locations, $\mathbf{r}$, where trajectories range over five or more time steps. Using an interpolation scheme, which is based on a series of the M'4 formula (Monaghan 1985) the Lagrangian quantities $\mathbf{u}(\mathbf{r})$ and $\mathbf{a}(\mathbf{r})$ are interpolated on a regular grid of 16^3 cells occupying a volume of 15^3 mm^3 into a Eulerian frame of reference. This results in differentiable, interpolated and time dependent velocity and acceleration fields which are smooth in regions with low particle seeding density and well resolved down to the Kolmogorov scale, η, in regions where the particle seeding density is high enough. All results presented here are taken from points only that have a 'relative divergence', defined by expression (1), smaller than 0.1.

$$\frac{div\mathbf{u}}{|\partial u_1/\partial x_1| + |\partial u_2/\partial x_2| + |\partial u_3/\partial x_3|} < 0.1 \qquad (1)$$

Typically 15% (~ 600 grid points/time step) of the regular grid points and 15% (~ 40 particle points/time step) of the particle points meet this criteria. Results denoted with $M'4$ refer to the procedure described above, whereas the subscript PTV denotes results obtained directly from 3D-PTV.

RESULTS

We note here that all the following results are in good agreement - both qualitatively and in many ways quantitatively - with those known from other physical and numerical experiments, see Kholmyansky et al. (2001a,b) and Tsinober et al. (2001) and references therein.

Accelerations and related matters

In order to check the validity of the interpolation scheme we start with a comparison between Lagrangian velocities, $\mathbf{u}_{PTV}$, and accelerations, $\mathbf{a}_{PTV}$, obtained directly from 3D-PTV data and the same quantities, $\mathbf{u}_{M'4}$, $\mathbf{a}_{M'4}$, in the Eulerian frame of reference obtained from M'4 interpolation. Since the rate of dissipation of kinetic energy, ε, can be calculated from $\varepsilon = -\langle \mathbf{u} \cdot \mathbf{a} \rangle$ (Ott and Mann 2000), one can expect that both, the probability density function (PDF) of $\mathbf{u} \cdot \mathbf{a}$ and the PDF of $\cos(\mathbf{u} \cdot \mathbf{a})$ are negatively skewed as it is clearly visible in figures 2 and 3. From the similar

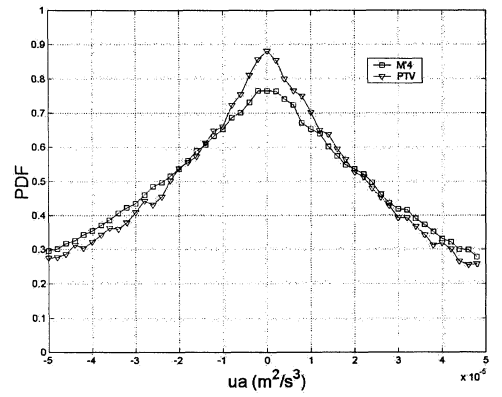

Figure 2: PDF of $u \cdot a$ showing a strongly non-Gaussian distribution.

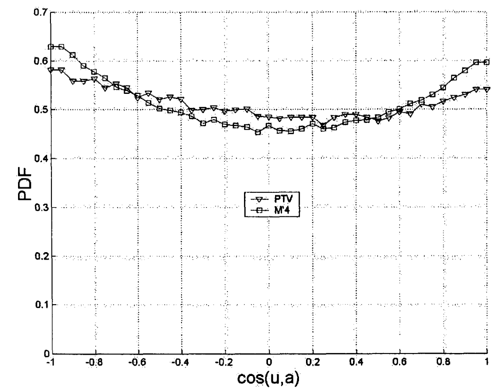

Figure 3: PDF of $\cos(u, a)$ for PTV and M'4 results.

behavior of both PDF's reasonable agreement between PTV and M'4 results is concluded. Moreover, the PDF's of $\cos(\mathbf{u} \cdot \mathbf{a})$ show large parallel and anti-parallel alignments and relatively small correlations between $\mathbf{u}$ and $\mathbf{a}$. For these reasons we can, at best, hope for order of magnitude accuracy for the value of ε. Table 1 shows values for the dissipation rate evaluated from $-\langle \mathbf{u} \cdot \mathbf{a} \rangle$ for PTV and M'4 compared with the value obtained from $2\nu \langle s_{ij} s_{ij} \rangle$ based on M'4, where $s_{ij} = 1/2(\partial u_i/\partial x_j + \partial u_j/\partial x_i)$ is the rate of strain tensor (see Tennekes and Lumley 1972).

From the average of these values, $\varepsilon \simeq 5 \cdot 10^{-6}$, characteristic turbulence scales of the flow can be calculated, namely the Kolmogorov length and time scales, $\eta = (\nu^3/\varepsilon)^{1/4}$ and $\tau_\eta = (\nu/\varepsilon)^{1/2}$ as $\eta \simeq 0.7mm$ and $\tau_\eta \simeq 0.5s$ respectively, the Taylor microscale, $\lambda_\tau = (15\nu \langle u_i^2 \rangle / \varepsilon)^{1/2}$ as $\lambda_\tau \simeq 7mm$ and with $u_0 = (1/3 \langle u_i^2 \rangle)^{1/2}$ as characteristic velocity, $u_0 = 0.01\ m/s$, we get the Taylor mi-

ε	$-\langle u\cdot a\rangle_{PTV}$	$-\langle u\cdot a\rangle_{M'4}$	$2\nu\langle s_{ij}s_{ij}\rangle$
m^2/s^3	5.8·10-6	3.2·10-6	6.2·10-6

Table 1: Dissipation rate ε evaluated from $-\langle ua\rangle$ and $2\nu\langle s_{ij}s_{ij}\rangle$.

croscale Reynolds number, $Re_\lambda = u_0\lambda_T/\nu$ as $Re_\lambda \simeq 60$. The total (Lagrangian) acceleration, $\mathbf{a} = D\mathbf{u}/Dt$, can be expressed by the local acceleration, $\mathbf{a}_l = \partial\mathbf{u}/\partial t$, and the convective acceleration, $\mathbf{a}_c = (\mathbf{u}\cdot\nabla)\mathbf{u}$, in the Eulerian frame of reference. Figure 4 shows the PDF of the cosine of the angle between local and convective acceleration. The strong tendency for anti-alignment due to mutual (statistical) cancellation between $\mathbf{a}_l$ and $\mathbf{a}_c$ is seen quite clearly by the strong negative skew of the PDF. One

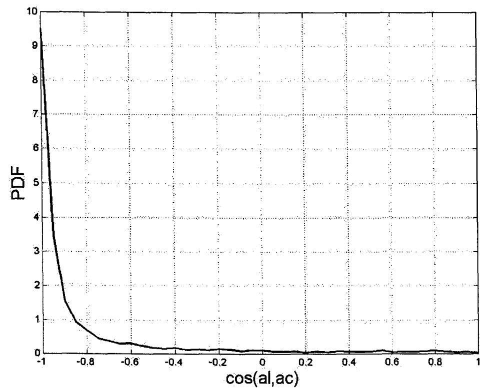

Figure 4: PDF of $\cos(a_l, a_c)$ showing strong anti-alignment between a_l and a_c.

more manifestation of the strong cancellation between $\mathbf{a}_l$ and $\mathbf{a}_c$ is a smaller intensity and a distribution of $\mathbf{a}$ more close to a Gaussian as compared to $\mathbf{a}_l$ and $\mathbf{a}_c$ (table 2, figure 5).

	$\langle a\cdot a\rangle$	$\langle a_l\cdot a_l\rangle$	$\langle a_c\cdot a_c\rangle$
m^2/s^4	2.1·10-4	4.2·10-4	5.8·10-4

Table 2: Lagrangian, local and convective mean accelerations.

These results are in good agreement with those obtained in field experiments (Kholmyansky et al. 2001a,b) and via DNS (Tsinober et al. 2000).

Vorticity and strain related quantities and relations

The rate of strain tensor s_{ij} can be expressed by its eigenvectors, λ_i, and their corresponding eigenvalues, Λ_i, where $\Lambda_1 > \Lambda_2 > \Lambda_3$. The PDF's of the Λ_i are shown in figure 6. The result is consistent with recent results obtained by Kholmyansky et al. (2001a,b) and references therein. We especially mention the typical PDF of the intermediate eigenvalue, Λ_2, which is distinctly positively skewed.

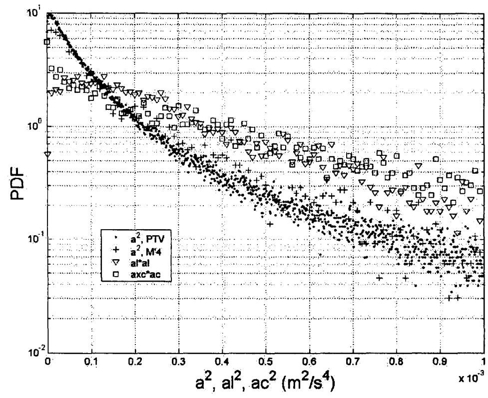

Figure 5: PDF of $a\cdot a_{PTV}$, $a\cdot a_{M'4}$, $a_l\cdot a_l$ and $a_c\cdot a_c$.

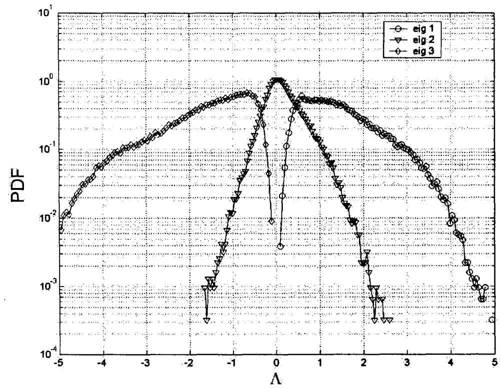

Figure 6: PDF's of the eigenvalues of the rate of strain tensor, s_{ij} , Λ_1, Λ_2 and Λ_3 (showing the positively skewed distribution of Λ_2).

Figure 7 shows the skewed PDF's of enstrophy, $\boldsymbol{\omega}^2$, production, with the vorticity of the velocity field, $\boldsymbol{\omega} = curl\ \mathbf{u}$, and strain production terms, $\omega_i\omega_j s_{ij}$ and $-4/3 s_{ij}s_{jk}s_{ki}$.

Although they are skewed similarly, their relationship is nonlocal as is seen from their joint PDF/scatter plot (figure 8).

The so called $R-Q$ joint PDF/scatter plot is shown in figure 9.

Here, $Q = 1/4\{\omega^2 - 2s^2\}$, and $R = -1/3\{s_{ij}s_{jk}s_{ki} + (3/4)\omega_i\omega_j s_{ij}\}$ are the second and the third invariants of the velocity gradient tensor $\partial u_i/\partial x_k$. A typical 'tear drop' pattern, similar to that obtained from numerical simulations, e.g. Martin et al. (1998) and Chacin and Cantwell (2000), is obtained from the experimental data.

Vorticity versus strain

One of the basic manifestations of preferential vortex stretching over vortex compression is the positive rate of enstrophy production, $\langle\omega_i\omega_j s_{ij}\rangle > 0$, shown in figure 7. It results from the preferential alignment between $\boldsymbol{\omega}$ and

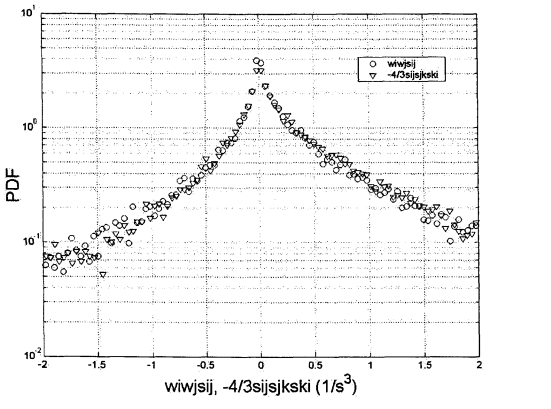

Figure 7: PDF's of $\omega_i\omega_j s_{ij}$ and $-4/3\ s_{ij}s_{jk}s_{ki}$ showing similar behavior.

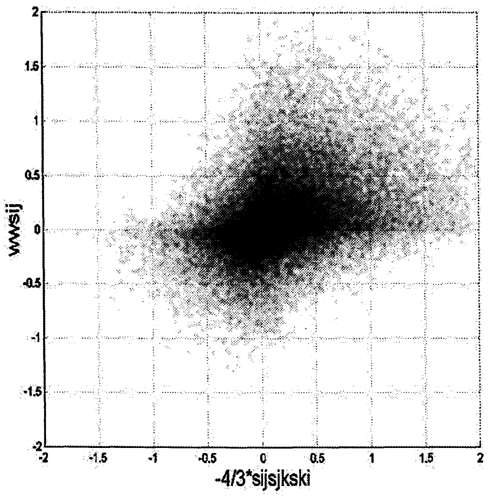

Figure 8: Joint PDF/scatter plot of $\omega_i\omega_j s_{sij}$ and $-4/3 s_{ij}s_{jk}s_{ki}$ showing strong non-locality.

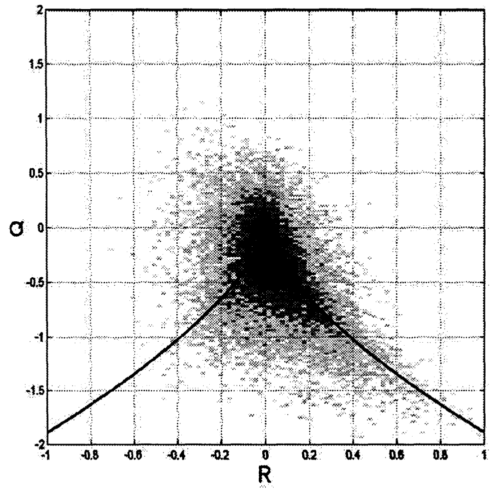

Figure 9: The $R - Q$ joint PDF/scatter plot with the discriminant, D, of A_{ij} equal to zero, $D = (27/4)R^2 + Q^3$.

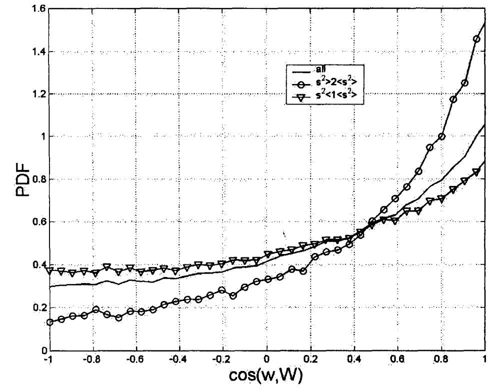

Figure 10: PDF's of the cosine of the angle between vorticity and the vortex stretching vector, $\cos(\boldsymbol{\omega}, \mathbf{W})$.

the vortex stretching vector, $\mathbf{W} = \omega_j s_{ij}$. Figure 10 shows that the PDF of $\cos(\boldsymbol{\omega}, \mathbf{W})$ is indeed strongly positively skewed. Moreover, the rate of enstrophy production, $\omega_i\omega_j s_{ij}$, becomes stronger in regions of higher strain, $s^2 > 2\langle s^2\rangle$ and it remains positive even in regions with low strain, $s^2 < \langle s^2\rangle$ in agreement with previous results, see Kholmyansky et al. (2001a,b) and references therein.

The alignments between vorticity, $\boldsymbol{\omega}$, and the eigenframe, $\boldsymbol{\lambda}_i$, of the rate of strain tensor s_{ij} are shown in figure 11 and again exhibit the well known strong tendency for alignment between $\boldsymbol{\omega}$ and the eigenvector $\boldsymbol{\lambda}_2$, corresponding to the intermediate eigenvalue, Λ_2. The combined effect of the alignments between $\boldsymbol{\omega}$ and $\boldsymbol{\lambda}_i$ and the behavior of Λ_i leads to quite peculiar contributions to the mean enstrophy production $\langle\omega_i\omega_j s_{ij}\rangle$ from the three terms associated with each Λ_i, $\omega_i\omega_j s_{ij} = \omega^2\Lambda_k \cos^2(\boldsymbol{\omega}, \boldsymbol{\lambda}_k)$ (table 3).

The largest contribution to $\langle\omega_i\omega_j s_{ij}\rangle$ is associated with the first term, Λ_1, in spite of the preferential alignment between $\boldsymbol{\omega}$ and $\boldsymbol{\lambda}_2$. This can be explained by the facts that the magnitude of Λ_2 is much smaller than the magnitude of $\Lambda_1$and that the eigenvalue Λ_2 takes both positive and negative values (figure 6) (Kholmyansky et al. 2001a). Similarly the largest contribution to vortex stretching $\langle\mathbf{W}^2\rangle$ comes also from the term associated with Λ_1 (table 3).

Material elements versus vorticity and strain.

It is well known that there is a preferential material line stretching in any (not necessarily real, e.g. Gaussian) random velocity field, see references in Tsinober (2001). This is shown by the positive value of $\langle r_i r_j s_{ij}/r^2\rangle$ given in table 4. Also in table 4 the values for the rates of relative vortex line stretching are given for the mean, weak and high intensities of vorticity.

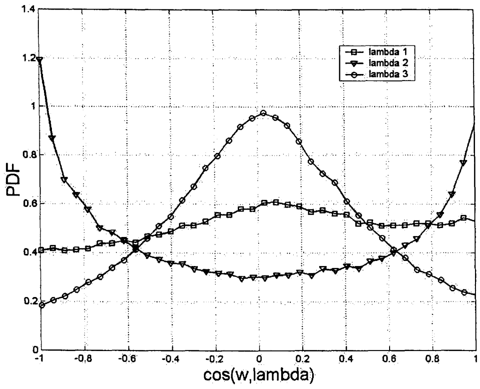

Figure 11: PDF's of the cosine of the angle between $\boldsymbol{\omega}$ and the eigenvectors $\boldsymbol{\lambda}_i$.

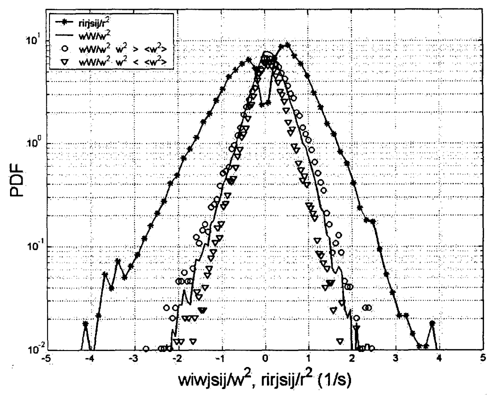

Figure 12: PDF's of realtive vortex- and material line stretching ($\omega_i\omega_j s_{ij}/\omega^2$, $r_i r_j s_{ij}/r^2$).

$\langle \omega^2\Lambda_1\cos^2(\omega,\lambda_1)\rangle$	$\langle \omega^2\Lambda_2\cos^2(\omega,\lambda_2)\rangle$	$\langle \omega^2\Lambda_3\cos^2(\omega,\lambda_3)\rangle$
1.79	0.50	-1.29
$\langle \omega^2\Lambda_1^2\cos^2(\omega,\lambda_1)\rangle$	$\langle \omega^2\Lambda_2^2\cos^2(\omega,\lambda_2)\rangle$	$\langle \omega^2\Lambda_3^2\cos^2(\omega,\lambda_3)\rangle$
0.50	0.11	0.39

Table 3: Contributions of terms associated with Λ_i to mean enstrophy production and vortex stretching vector.

$\langle \frac{\omega_i\omega_j s_{ij}}{\omega^2} \rangle$	*all*	$\omega < \langle\omega\rangle$	$\omega > \langle\omega\rangle$	$\langle \frac{r_i r_j s_{ij}}{r^2} \rangle$
s^{-1}	0.09	0.06	0.13	0.07

Table 4: Relative vortex and material line stretching.

As all values of table 4 are positive, the PDF's of the same quantities shown in figure 12 are also (slightly) positively skewed just like the PDF of $\cos(\mathbf{r},\mathbf{W}^r)$, $W_i^r = r_j s_{ij}$ shown in figure 13.

Moreover, the PDF's of $r_i r_j s_{ij}$ and $\cos(\mathbf{r},\mathbf{W}^r)$ show a distinct compression and stretching region and strong anti-parallel and parallel alignment respectively. Thus they differ significantly from the PDF's of $\omega_i\omega_j s_{ij}$ and $\cos(\boldsymbol{\omega},\mathbf{W})$ which do not show this bimodal characteristic but have only a tendency towards stretching and parallel alignment.

A new aspect of material line stretching is shown in the PDF's of $cos(\mathbf{r},\boldsymbol{\lambda}_i)$ (figure 14). Strong tendencies for alignment are observed between $\mathbf{r}$ and the eigenvectors $\boldsymbol{\lambda}_1$and $\boldsymbol{\lambda}_3$. The two minima of the PDF's of $cos(\mathbf{r},\boldsymbol{\lambda}_1)$ and $cos(\mathbf{r},\boldsymbol{\lambda}_3)$ and the strong normal orientation between $\mathbf{r}$ and $\boldsymbol{\lambda}_2$ suggest an almost 'binary' state of $\mathbf{r}$, being either stretched or compressed. This is in contrast with the alignment of $\boldsymbol{\omega}$ with the eigenframe $\boldsymbol{\lambda}_i$ shown in figure 11 where the strongest alignment is observed between $\boldsymbol{\omega}$ and $\boldsymbol{\lambda}_2$.

Vortex lines are dynamically active. Their behavior is different from that of material lines, even when they are identical at one instant of time. A vortex line and a material line which initially are aligned, disalign faster than two

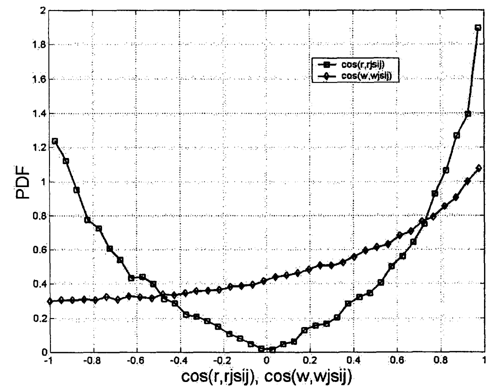

Figure 13: PDF's of $\cos(\mathbf{r},\mathbf{W}^r)$ and $\cos(\boldsymbol{\omega},\mathbf{W})$.

material lines. With α as the angle between a vortex line and a material line and β as the angle between two material lines respectively, this is demonstrated in figure 15 showing a stronger rate of change of α, $||D\alpha/Dt||$, compared to the rate of change of β, $||D\beta/Dt||$, regardless of the initial alignment.

CONCLUDING REMARKS

We have demonstrated that there is a large potential in using the 3D-PTV technique in studying rather subtle physical effects in turbulent flows associated with the field of velocity derivatives. The main difference as compared to 'conventional' approaches is that one goes in the 'reverse' direction starting with a Lagrangian raw data set and deducing from it the Eulerian flow properties. The Lagrangian starting point will allow a monitoring of geometrical relations and quantities, such as enstrophy, strain and their production rates, along particle trajectories, as well as tracing of vortex and material lines in time. This requires however a higher quality of the raw data. Therefore, the next task to be addressed in the

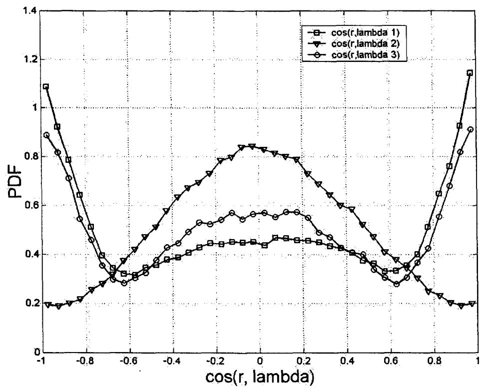

Figure 14: PDF's of cosines of the angles between $\mathbf{r}$ and eigenvectors $\boldsymbol{\lambda}_i$.

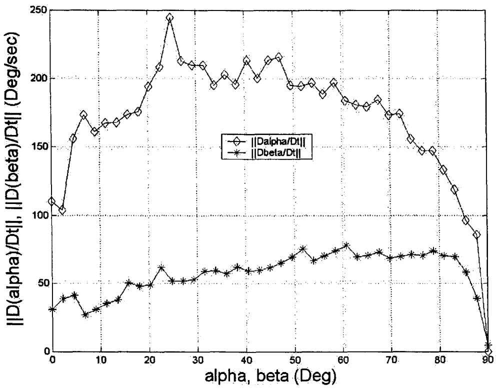

Figure 15: The range of 90° was divided into 40 slots. For each slot the average of the rate of change of the angle α and β was taken and plotted over their initial alignment, where α is the angle between a vortex and a material line and β is the angle between two material lines respectively.

wake of this work is a more detailed classification and characterization of the formed particle clusters for which generally higher spatial resolutions can be obtained.

REFERENCES

Chacin, J. M., Cantwell, B. J. (2000) Dynamics of a low Reynolds number turbulent boundary layer, *J. Fluid Mech.*, **404**, 87 - 115.

Kholmyansky, M., Tsinober, A. and Yorish, S. (2001a) Velocity derivatives in the atmospheric surface layer at $Re_\lambda = 10^4$, *Phys. Fluids*, **13**, 311-314.

Kholmyansky, M., Tsinober, A. and Yorish, S. (2001b) Velocity derivatives in the atmospheric surface layer at $Re_\lambda = 10^4$, *this issue.*

Kolmogorov, A. N. (1941) Dissipation of energy in locally isotropic turbulence, *Dokl. Akad. Nauk SSSR*, **32,** 19 - 21.

Martin, J. N., Ooi, A., Chong, M. S. and Soria, J. (1998) Dynamics of the velocity gradient tensor invariants in isotropic turbulence, *Phys. Fluids*, **10**, 2336 - 2346.

Monaghan, J. J. (1985) Particle methods for hydrodynamics, *Comput. Phys. Rep.*, **3**, 71-124.

Ott, S. and Mann, J. (2000) An experimental investigation of the relative diffusion of particle pairs in three dimensional turbulent flow, *J. Fluid. Mech.*, **422**, 207 - 223.

Stüer, H., Maas, H.-G., Virant, M., Becker, J. (1999) A volumetric 3D measurement tool for velocity field diagnostics in microgravity experiments, *Meas. Sci. Technol.* **10**, 904 - 913.

Taylor, G. I. (1938) Production and dissipation of vorticity in a turbulent fluid, *Proc. Roy. Soc.*, **A164**, 15 - 23.

Tennekes, H. and Lumley, J. L. (1972) A first course in turbulence, *The MIT Press*, 59-75.

Tsinober, A., Yeung, P. K. and Vedula, P. (2000) Random Taylor hypothesis and geometrical statistics of local and convective accelerations in isotropic turbulence, *Phys. Fluids*, to be published.

Tsinober, A. (2001) An informal introduction to turbulence, *Kluwer*, to be published.